Structural analysis of substrate binding by the TatBC component of the twin-arginine protein transport system

Michael J. Tarry[a,1,2], Eva Schäfer[b,1,3], Shuyun Chen[a], Grant Buchanan[c], Nicholas P. Greene[a], Susan M. Lea[d], Tracy Palmer[c], Helen R. Saibil[b,4], and Ben C. Berks[a,4]

[a]Department of Biochemistry, University of Oxford, South Parks Road, Oxford OX1 3QU, United Kingdom; [b]Department of Crystallography and Institute of Structural and Molecular Biology, Birkbeck College London, Malet Street, London WC1E 7HX, United Kingdom; [c]Division of Molecular and Environmental Microbiology, College of Life Sciences, University of Dundee, Dundee DD1 5EH, United Kingdom; and [d]Sir William Dunn School of Pathology, University of Oxford, South Parks Road, Oxford OX1 3RE, United Kingdom

Edited by Linda L. Randall, University of Missouri, Columbia, MO, and approved June 4, 2009 (received for review February 12, 2009)

The Tat system transports folded proteins across the bacterial cytoplasmic membrane and the thylakoid membrane of plant chloroplasts. In *Escherichia coli* substrate proteins initially bind to the integral membrane TatBC complex which then recruits the protein TatA to effect translocation. Overproduction of TatBC and the substrate protein SufI in the absence of TatA led to the accumulation of TatBC-SufI complexes that could be purified using an affinity tag on the substrate. Three-dimensional structures of the TatBC-SufI complexes and unliganded TatBC were obtained by single-particle electron microscopy and random conical tilt reconstruction. Comparison of the structures shows that substrate molecules bind on the periphery of the TatBC complex and that substrate binding causes a significant reduction in diameter of the TatBC part of the complex. Although the TatBC complex contains multiple copies of the signal peptide-binding TatC protomer, purified TatBC-SufI complexes contain only 1 or 2 SufI molecules. Where 2 substrates are present in the TatBC-SufI complex, they are bound at adjacent sites. These observations imply that only certain TatC protomers within the complex interact with substrate or that there is a negative cooperativity of substrate binding. Similar TatBC-substrate complexes can be generated by an alternative in vitro reconstitution method and using a different substrate protein.

membrane protein | *Escherichia coli* | blue native PAGE | single particle electron microscopy

The twin arginine translocation (Tat) system transports folded proteins across the cytoplasmic membrane of prokaryotes and the thylakoid membrane of plant chloroplasts (1–4). The Tat pathway is involved in a wide range of cellular functions including biosynthesis of respiratory and photosynthetic electron transfer chains, formation of the bacterial cell envelope, bacterial motility, establishment of the nitrogen-fixing symbiosis, quorum sensing, and bacterial pathogenesis (5, 6). The task faced by the Tat system is mechanistically very challenging because it involves transporting large protein substrates of differing size and surface properties across a membrane while maintaining the membrane permeability barrier. Proteins are targeted to the Tat system by N-terminal signal peptides bearing a consensus amino acid motif that contains consecutive arginine residues (7, 8). Transport through the Tat pathway is energized by the transmembrane proton electrochemical gradient (9).

The minimal components of the Tat system in the bacterium *Escherichia coli* are the 3 integral membrane proteins TatA, TatB, and TatC (10–13). TatB and TatC are found in a large complex containing multiple copies of each of the 2 constituent subunits (14–16). This TatBC complex acts as the membrane receptor of the Tat system with the twin arginine motif of the substrate signal peptide being specifically recognized by the TatC subunit (17–19). TatA forms homo-oligomeric ring-like structures of variable size that are likely to constitute the protein translocating channels of the Tat system (20, 21). Current models of the Tat transport cycle propose that substrate proteins initially bind to TatBC which then recruits TatA to form the active translocation complex (18, 21–24).

This study reports the trapping and isolation of *E. coli* TatBC-substrate complexes and their structural characterization by electron microscopy. Structures of the unliganded TatBC complex were also determined for comparison. This study presents 3-dimensional structural information on TatBC complexes and provides significant insights into the way the TatBC complex interacts with substrate proteins.

Results

Isolation and Biochemical Characterization of TatBC-substrate Complexes. Complexes between TatBC and the native *E. coli* Tat substrate SufI (a cell division protein; 25) were generated in vivo by coordinately overproducing SufI and TatBC in a strain lacking other Tat components. The TatBC-SufI intermediate accumulates under these conditions because it is unable to progress further through the transport cycle in the absence of TatA (and its paralogue TatE). The SufI precursor protein was engineered with a C-terminal hexahistidine tag to allow the specific isolation of substrate-bound TatBC complexes.

Membranes from cells overproducing TatBC and $SufI_{His}$ were solubilized in digitonin, a detergent that is known to maintain the integrity of the TatBC complex (16). The resulting soluble extract was subjected to Ni^{2+}-affinity chromatography. Fractions eluted from the affinity matrix with an imidazole gradient contained $SufI_{His}$, TatB, and TatC (Fig. S1). Since only the SufI protein possesses a polyhistidine affinity tag it can be inferred that the TatB and TatC proteins are retained by the column because they are bound to SufI. A control experiment confirmed that TatB and TatC did not bind to the Ni^{2+}-affinity column in the absence of $SufI_{His}$.

The TatBC-$SufI_{His}$ complexes present in the Ni^{2+}-affinity

Author contributions: M.J.T., E.S., S.M.L., T.P., H.R.S., and B.C.B. designed research; M.J.T., E.S., and S.C. performed research; N.P.G., G.B., and T.P. contributed new reagents/analytic tools; E.S. analyzed data; and M.T., E.S., S.M.L., T.P., H.R.S., and B.C.B. wrote the paper.

The authors declare no conflict of interest.

This article is a PNAS Direct Submission.

Freely available online through the PNAS open access option.

[1]M.J.T. and E.S. contributed equally to this work.

[2]Present address: Center for Biomembrane Research, Department of Biochemistry and Biophysics, Stockholm University, SE-106 91 Stockholm, Sweden.

[3]Present address: Max Planck Institute of Biophysics, Max-von-Laue-Strasse 3, 60438 Frankfurt am Main, Germany.

[4]To whom correspondence may be addressed. E-mail: ben.berks@bioch.ox.ac.uk or h.saibil@mail.cryst.bbk.ac.uk.

This article contains supporting information online at www.pnas.org/cgi/content/full/0901566106/DCSupplemental.

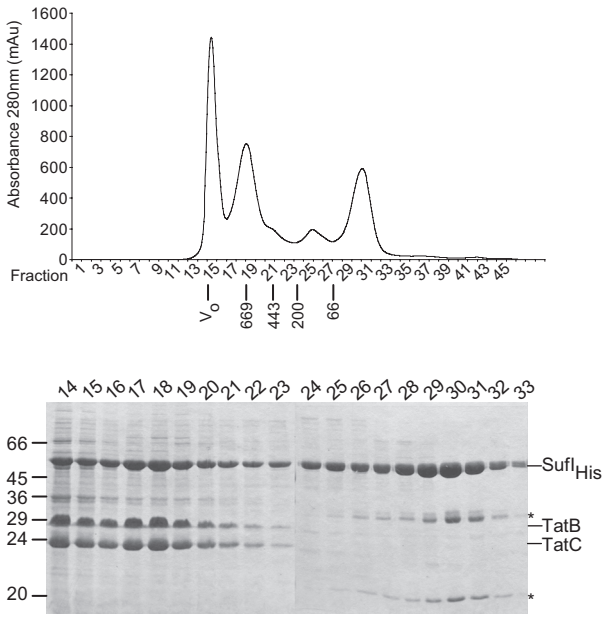

Fig. 1. Purification of a complex between TatBC and the Tat substrate SufI. TatBC and a modified version of the SufI precursor protein possessing a C-terminal hexa-histidine tag were coordinately overexpressed in the Δ*tatABCD*Δ*tatE* strain DADE. Membranes were isolated, solubilized in digitonin, and subjected to Ni^{2+}-affinity chromatography. The peak TatBC-containing fractions from the Ni^{2+} affinity column were pooled, concentrated, and applied to a size exclusion chromatography column. (Top) The 280 nm absorbance profile of the eluant. The void volume (V_0) and elution positions of water soluble standard proteins are indicated below the profile. (Bottom) The proteins present in successive indicated fractions eluting from the size exclusion column are analyzed by SDS/PAGE and Coomassie Blue staining. The molecular masses in kDa of standard proteins are given to the left of each gel and the positions of SufI, TatB and TatC to the right of each gel. SufI degradation products are indicated by (*).

column eluant were separated from free $SufI_{His}$ by size exclusion chromatography (Fig. 1). TatB and TatC coeluted with $SufI_{His}$ in a peak corresponding to an apparent molecular mass of 670 kDa. N-terminal sequencing showed that the unprocessed (but lacking the initiator methionine) precursor form of $SufI_{His}$ was present in these TatBC-$SufI_{His}$ complexes. Free $SufI_{His}$ was found in a peak with an apparent molecular mass of <50 kDa corresponding to the elution position of mature $SufI_{His}$. Two SufI degradation products previously identified as arising from proteolysis of a long surface loop (25) copurified with free $SufI_{His}$. The SufI protein present in the TatBC-$SufI_{His}$ complexes does not exhibit this proteolytic event suggesting that access to this region of $SufI_{His}$ is protected in the complexes.

The composition of the TatBC-$SufI_{His}$ preparation was analyzed by blue native-PAGE (Fig. 2*A*). Three species with apparent molecular masses of 500, 540, and 580 kDa were resolved. Insight into the composition of the 3 species was provided by subjecting the sample to a second Ni^{2+}-affinity chromatography experiment. The 500-kDa species did not bind to the column and was found to contain TatB and TatC but not $SufI_{His}$ (Fig. 2 *B* and *C*). The 500-kDa complex, therefore, corresponds to TatBC that has released $SufI_{His}$ subsequent to the first Ni^{2+}-affinity step. This dissociation can be inferred to be an ongoing process during isolation because the 500 kDa species was also found in the fraction subsequently eluted from the column with 150 mM imidazole (Fig. 2*D*). The 500-kDa TatBC complex has a higher apparent molecular mass than the $TatBC_{His}$ complex purified in the same detergent (Fig. 2*A*), suggesting that the presence of a hexahistidine tag has a significant effect on the mobility of the TatBC complex under blue native-PAGE. The $SufI_{His}$-containing complexes bound to the second Ni^{2+}-affinity column could be partially resolved by step elution with different concentrations of imidazole (Fig. 2 *B* and *D*). Complexes eluting at a lower imidazole concentration contained predominantly the 540-kDa species, whereas those eluting at a higher imidazole concentration corresponded to the 580-kDa species (Fig. 2*D*). The higher affinity of the 580-kDa species for the Ni^{2+}-affinity column suggests that this complex contains more hexahistidine tags, and thus more copies of $SufI_{His}$, than the 540-kDa species. Because the 500-kDa species does not contain $SufI_{His}$, and the molecular mass of the $SufI_{His}$ precursor is 53 kDa, the 540-kDa species is most likely to bind 1, and the 580-kDa species 2, $SufI_{His}$ molecules.

Electron Microscopy of TatBC and TatBC-Substrate Complexes. Samples of the TatBC-$SufI_{His}$ complexes were analyzed by single-particle electron microscopy. For comparison $TatBC_{His}$ complexes purified by a similar protocol were also analyzed. For both samples, the particles had a preferred orientation on the carbon support. A random conical tilt approach (26) was therefore used to determine 3-D maps of $TatBC_{His}$ and TatBC-$SufI_{His}$. In total, 2,885 particles were selected from 11 tilt pairs of the TatBC sample and 5,682 particles from 35 tilt pairs of the TatBC-SufI preparation.

$TatBC_{His}$. The particles from the $TatBC_{His}$ sample were sorted into 150 classes, some of which are shown in Fig. 3 *A* and *B*. The particles are slightly elongated, with a maximum length of 10–12 nm and a spiky border (Fig. 3 *A* and *B*). Three-dimensional maps of the different classes were calculated and similar ones were combined. This processing resulted in 2 3-D maps, a smaller one (Fig. 4*A*, 1,358 images) derived from the data shown in Fig. 3*A*, and a larger one (Fig. 4*B*, 911 images) from the data in Fig. 3*B*. Both maps have a roughly hemispherical shape. The isosurface threshold was chosen to include all of the strong density but exclude noise features. These surfaces enclose volumes consistent with the molecular mass determined by blue native-PAGE analysis (Fig. 2*A*). At the threshold shown, the bigger 3-D map has a molecular mass of approximately 420 kDa and the smaller 3-D map a molecular mass of approximately 380 kDa, assuming a protein density of 844 Da/nm^3.

The approximate 50-Å height of the $TatBC_{His}$ hemisphere (Fig. 4 *A* and *B*) is compatible with the thickness of a lipid bilayer. We propose that TatBC is positioned in the membrane such that the plane of the $TatBC_{His}$ hemisphere is parallel to the plane of the lipid bilayer as shown in the right hand side of Fig. 4*A*. Only in this orientation would the face of the particle contacting the carbon support be distinct from the opposite surface (cytoplasmic versus periplasmic face or vice versa), leading to the observed unique orientation of the particles on the carbon support.

TatBC-$SufI_{His}$ Complexes. Raw images of the TatBC-$SufI_{His}$ preparation showed particles of ≈10-nm diameter, some of which had small protrusions (Fig. S2 *A* and *B*). The images of the TatBC-$SufI_{His}$ complex were classified into 3 approximately equal subsets on the basis of these additional features. One subset (1,556 images) (Fig. 3*C*) strongly resembled the $TatBC_{His}$ complex alone (Fig. 3 *A* and *B*). These particles are likely to be TatBC with no substrate bound. Because these TatBC complexes do not possess a His-tag it can be inferred that the presence of a His-tag on the C terminus of TatC does not change the overall structure of the TatBC complex. The second subset (1,297 images) displayed a 9.5–11-nm diameter round density with a single protrusion of approximately 4.5 nm in length (Fig. 3*D*). The third subset (1,284 images) displayed a similar round density but with 2 protrusions (Fig. 3*E*). Since the protrusions are approximately the size of a SufI monomer, it is very likely that each protrusion corresponds to 1 $SufI_{His}$ molecule and that the

BIOCHEMISTRY

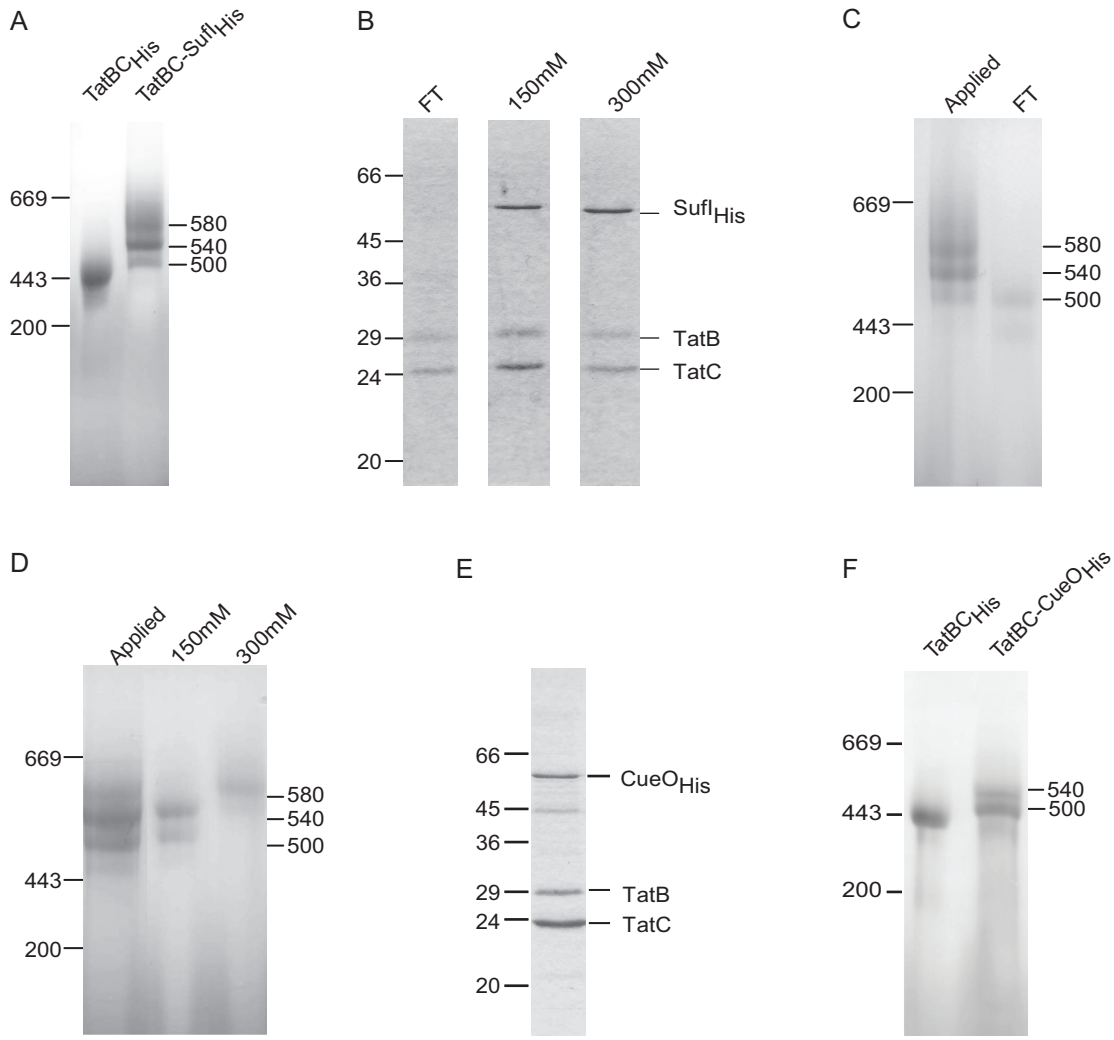

Fig. 2. Biochemical analysis of purified TatBC-substrate complexes. (*A*) Blue native-PAGE analysis of the TatBC-SufI$_{His}$ preparation and of purified TatBC$_{His}$. (*B*) The TatBC-SufI$_{His}$ preparation was applied to a Ni^{2+}-affinity chromatography column and bound proteins eluted with washes at 150 mM and 300 mM imidazole. SDS/PAGE analysis of proteins that did not bind to the column (FT) and of bound proteins that were eluted from the column by the 150 mM and 300 mM imidazole steps. (*C*) Blue native-PAGE analysis of the TatBC-SufI$_{His}$ preparation that was applied to the Ni^{2+} affinity column (Applied) and the protein that did not bind to the column (FT). (*D*) Blue native-PAGE analysis of the TatBC-SufI$_{His}$ preparation that was applied to the Ni^{2+} affinity column (Applied) and of the bound proteins eluted from the column by the 150 mM and 300 mM imidazole steps. (*E*) SDS/PAGE analysis of the TatBC-CueO$_{His}$ preparation. (*F*) Bue native-PAGE analysis of the TatBC-CueO$_{His}$ preparation and purified TatBC$_{His}$. All gels were stained with Coomassie Brilliant Blue. The molecular masses (kDa) of standard proteins are given to the left of each gel. Protein complexes resolved by blue native-PAGE are labeled by molecular mass (kDa) to the right of the gels.

round central density is TatBC. Biochemical experiments (above) also suggested a distribution of TatBC complexes with 0, 1, or 2 SufI$_{His}$ molecules bound. It is notable that in the complexes with 2 protrusions, the protrusions are always closely adjacent (Fig. 3*E*).

Three-dimensional maps were calculated for TatBC-SufI$_{His}$ complexes with 1 or 2 SufI bound using all of the data for each subset. These structures are displayed in Fig. 4 *C* and *D* in the same orientation relative to the support film as the TatBC$_{His}$ complexes in Fig. 4 *A* and *B*. Density thresholds were chosen for the 3-D maps so that the mass of each protrusion corresponds to the 50-kDa mass of SufI. On this basis the TatBC component of the complexes has a molecular mass of approximately 350 kDa. Examination of individual class averages or the final 3-D maps shows that the TatBC part of the substrate complexes is noticeably smaller than TatBC alone (isolated either as TatBC$_{His}$ or in the unbound fraction of TatBC-SufI$_{His}$) (Fig. 3 *A–C*, Fig. 4 *A* and *B*, and Fig. S2 *C* and *D* versus Figs. 3 *D* and *E*, Fig. 4 *C* and *D*, and Fig. S2 *E* and *F*).

The X-ray structure of SufI (25) was fitted into the protrusions of the TatBC-SufI$_{His}$ complexes with the N terminus, containing the Tat signal peptide, contacting the TatBC complex (Fig. 4 *E* and *F*). The density assigned to SufI accommodates the X-ray structure very well in this orientation and is entirely consistent with SufI being in the fully folded state in the complex. The close approach of the SufI$_{His}$ densities to the TatBC core suggests that the 27-amino acid SufI signal peptide is predominantly buried in the adjacent TatBC complex.

The 3-D maps of the TatBC$_{His}$ and TatBC-SufI$_{His}$ complexes have resolutions of 3.5–4.5 nm. Central sections of the maps show that all of the 3-D structures have an internal cavity (Fig. 4*G* and Fig. S2 *C–F*). No connectivity between the internal cavity and the surface of the particles is apparent at the current resolution.

Characterization of TaBC-CueO$_{His}$ Complexes Produced by In Vitro Reconstitution. To assess the generality of the biochemical and structural conclusions derived from our studies of TatBC-SufI$_{His}$ complexes, we generated and characterized a second type of TatBC-substrate complex. This complex contained a different

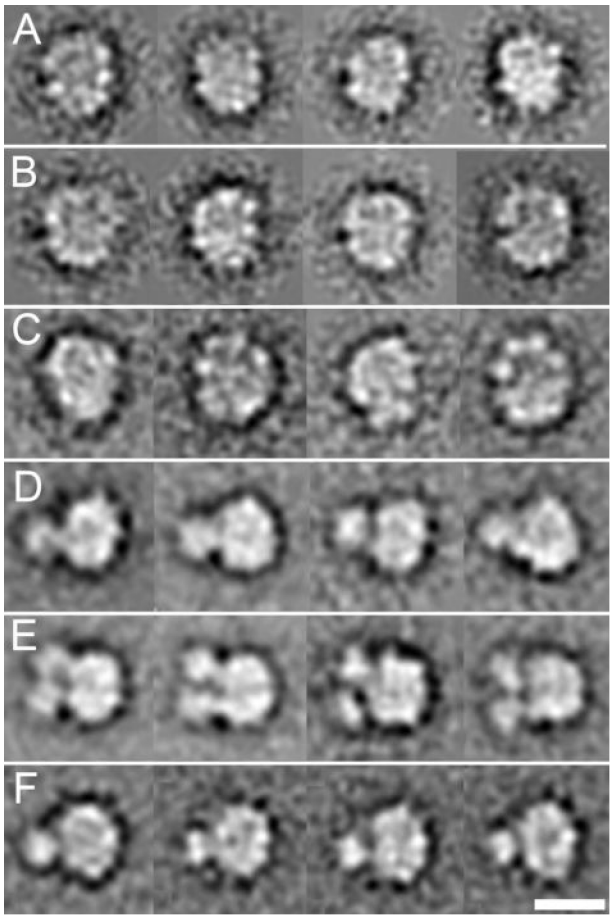

Fig. 3. Class averages of the TatBC complex with and without bound substrate. Class averages obtained by multireference alignment of the untilted images of $TatBC_{His}$, TatBC-$SufI_{His}$, and TatBC-$CueO_{His}$ samples. (*A*) The small $TatBC_{His}$ complex. (*B*) The large $TatBC_{His}$ complex. (*C*) The TatBC complex with no $SufI_{His}$ bound. (*D*) The TatBC complex with 1 $SufI_{His}$ bound. (*E*) The TatBC complex with 2 $SufI_{His}$ bound. (*F*) The TatBC complex with 1 $CueO_{His}$ bound. There were 15–25 images per class in each case. (Scale bar, 10 nm.)

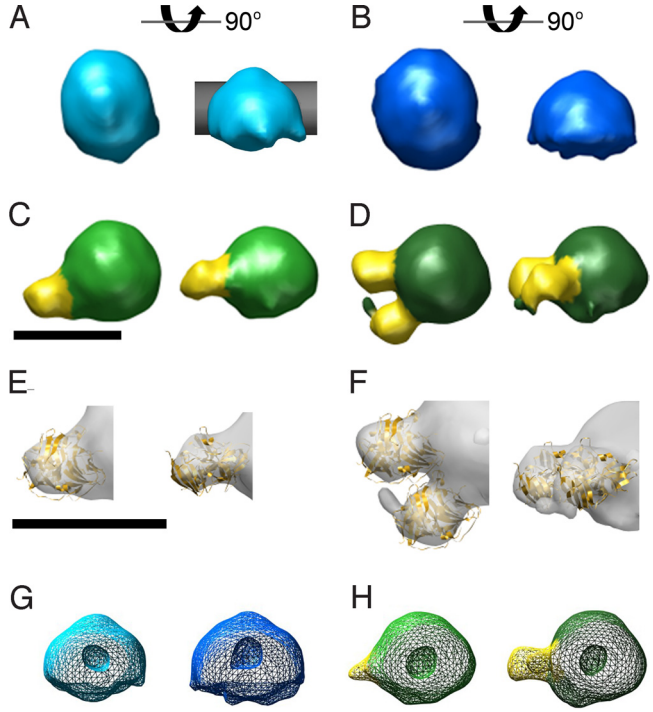

Fig. 4. 3D maps of $TatBC_{His}$ and TatBC-$SufI_{His}$ complexes. (*A*) The small $TatBC_{His}$ complex (light blue). (*B*) The large $TatBC_{His}$ complex (blue). (*C*) TatBC (green) with 1 $SufI_{His}$ (yellow) bound. (*D*) TatBC (green) with 2 $SufI_{His}$ (yellow) bound. Each map is shown in 2 orientations related by a 90 ° rotation about the horizontal axis. All maps are shown in the same orientation relative to the support film which is at the bottom in the right hand views. The gray box in *A* shows the possible location of the membrane. The X-ray structure of SufI (yellow) is fitted into the 3-D maps (gray) for the TatBC complex with 1 (*E*) or 2 (*F*) bound $SufI_{His}$ molecules. (*G*) From left to right, views of the small and large $TatBC_{His}$ complexes, and the TatBC complex with 1 and 2 bound $SufI_{His}$ molecules with the front surface cut away to reveal the internal cavity. The complexes are shown in the same orientation as the right hand views in panels (*A–D*). The map surfaces are shown as wire mesh with the back surface represented in darker colors. (Scale bars, 10 nm; larger scale bar applies to *E* and *F* only.)

substrate protein, the native *E. coli* Tat substrate CueO [a putative Cu(I) oxidase; (27)], prepared by an alternative in vitro reconstitution method. Inverted inner membrane vesicles (IMVs) were isolated from a strain overproducing TatBC but lacking other Tat components. The IMVs were then mixed with purified $CueO_{His}$ precursor in the presence of ATP to generate a transmembrane proton electrochemical gradient via ATP synthase. The IMVs were solubilized in digitonin and TatBC-$CueO_{His}$ complexes were purified in the same way as the TatBC-$SufI_{His}$ complexes (Fig. 2*E*). Analysis of the preparation by blue native-PAGE revealed complexes with molecular masses of 500 and 540 kDa (Fig. 2*F*). By analogy to the TatBC-$SufI_{His}$ preparation, these 2 species correspond to TatBC and TatBC bound to a single molecule of $CueO_{His}$. Control experiments using a transport-inactive variant of $CueO_{His}$ in which a lysine pair is substituted for the twin arginine residues of the signal peptide confirmed that a functional signal peptide was required to isolate TatBC-$CueO_{His}$ complexes.

The complexes in the TatBC-$CueO_{His}$ sample were analyzed by single-particle electron microscopy. From 26 CCD images, 4,998 particles were selected and processed. The dataset was divided into 2 subsets. One resembled TatBC alone. The other displayed a 10–11-nm diameter round density with a single protrusion of approximately 4.5 nm in length (Fig. 3*F*) resembling the TatBC-$SufI_{His}$ complexes with 1 SufI bound (Fig. 3*D*). The size of the protrusion is consistent with the structure of CueO determined by X-ray crystallography (28). Only 485 particles (<10%) show the protrusion bound to the TatBC particle. This observation is consistent with the low staining intensity of the 540-kDa species relative to the 500-kDa species on blue native-PAGE (Fig. 2*F*). As seen with the TatBC-$SufI_{His}$ complexes, the density attributed to TatBC in the TatBC-$CueO_{His}$ complexes is smaller than either of the substrate-free $TatBC_{His}$ complexes.

As a further control we determined the 3-D structures of $TatA_{His}$ complexes that had also been purified in digitonin (Fig. S3 and Fig. S4). These TatA structures are not significantly different from those previously determined for TatA in the detergent $C_{12}E_9$ (19) even though blue native PAGE only resolves distinct complexes for the latter preparation [compare Fig. S3*B* with Fig. 1*E* in ref. 19]. This observation shows that the gross structure of the TatA complex is not detergent-specific. Importantly the morphology of TatA in digitonin is clearly distinct from that of the TatBC complex in the same detergent, with the TatA complexes having a considerably larger internal cavity that is open to 1 face of the particle.

Discussion

We have used single-particle electron microscopy to obtain 3-D structures of the TatBC complex both in isolation and bound to

water-soluble substrate proteins. Importantly the structures of TatBC-substrate complexes formed by 2 different approaches (in vivo-assembled TatBC-$SufI_{His}$ and in vitro-assembled TatBC-$CueO_{His}$) revealed the same location of substrate on the TatBC complex and the same structural change on substrate binding in the TatBC part, arguing for the generality of our observations.

The TatBC-substrate structures show that the substrate proteins are located at the periphery of the TatBC complex. Although there is a cavity in the interior of the TatBC particle (Fig. 4*G* and Fig. S2 *C* and *D*), it is too small to accommodate a substrate of the size of SufI or CueO. In addition, the cavity has no obvious opening to the surface of the particle, and there is no evidence from the substrate-bound structures that the cavity either dilates or contains substrate (Fig. 4*G* and Fig. S2 *E* and *F*). Therefore, the structural data give no indication that the substrate molecule enters the interior of the TatBC complex during transport. Instead, as anticipated by some mechanistic models (17, 20, 29), the peripheral location of the substrate would be appropriate for interaction with TatA units recruited from the surrounding membrane to form the translocation pathway.

Comparison of the averaged images of TatBC with and without bound substrate shows that the TatBC part undergoes a major structural reorganisation with TatBC bound to substrate being significantly smaller than the unliganded complex (Fig. 3 *A–C*, Fig. 4 *A* and *B*, and Fig. S2 *C* and *D* versus Figs. 3 *D* and *F*, Fig. 4*C* and *D*, and Fig. S2 *E* and *F*). This difference cannot be accounted for solely by changes in subunit packing—the smaller structure does not appear more densely packed—and therefore implies a loss of subunits from the TatBC complex when substrate is bound. There is already considerable evidence that both the oligomeric state of TatA and its interaction with TatBC alter during the transport cycle (17, 18, 21–24), so our observations that TatBC can also change size suggest that protein–protein interactions in the entire Tat system are highly dynamic. It has been proposed that detergent extraction alters the equilibrium between TatA monomer and oligomer states found in the native membrane environment (20) and this possibility must also be borne in mind when considering the TatBC structures. The observed reorganization of TatBC upon substrate binding is consistent with the proposal that TatBC undergoes a substrate-dependent structural change to allow recruitment of TatA (17). Structural change in TatBC has also been invoked to explain a pmf-dependent tightening of the substrate-TatBC interaction in the thylakoid Tat system (30).

The TatBC complex contains multiple copies of the signal peptide-binding TatC protomer and would, therefore, be anticipated to contain multiple substrate binding sites. However, not more than 2 bound substrate molecules are seen in the TatBC-$SufI_{His}$ structures and only a single bound substrate is observed in the TatBC-$CueO_{His}$ structures. What could be the explanation for this substoichiometric occupancy of potential substrate binding sites? The concentration of $CueO_{His}$ used to generate the TatBC-$CueO_{His}$ complexes (18 μM) is significantly in excess of the apparent affinity of the TatBC complex for $CueO_{His}$ as determined by transport competition experiments ($K_i \approx 0.1$ μM; Fig. S5). Similarly, during in vivo generation of TatBC-$SufI_{His}$ complexes excess precursor protein accumulates in the soluble phase. Formation of TatBC-substrate complexes in our experiments should, therefore, be occurring close to substrate saturation and we would expect all functional substrate binding sites in TatBC to be occupied at the start of the purification procedure. With this scenario in mind possible explanations for the substoichiometric occupancy of substrate binding sites by TatBC are that the other binding sites are either not functional or bind substrate too weakly to allow isolation. There are 2 possible models to account for this behavior. In the first model, inherent asymmetry within the structure of the TatBC complex allows functional binding sites at only 1 or 2 specific positions. In the second model, all substrate binding sites are equally available but substrate binding is anti-cooperative. In the latter model binding of a substrate molecule at a randomly selected site induces a concerted structural change within the TatBC complex (as observed) and this change inhibits the interaction of substrate molecules with the remaining binding sites. Cooperative interactions between substrate binding sites in TatBC have previously been inferred for the chloroplast Tat system (31).

Although models invoking nonequivalence of substrate binding sites can explain the observed substoichiometric binding of substrate to TatBC, it is important to note that the identification of substrate-free TatBC complexes in the TatBC-substrate preparations (Fig. 2 *A–D* and *F*) shows that some TatBC-substrate complexes release all bound substrate molecules during purification. This observation raises the possibility that all substrate binding sites in TatBC are equivalent and functional but that the majority of the bound substrate molecules dissociate from the TatBC-substrate complex during purification. We do not favor this explanation for the low occupancy of the TatBC substrate binding sites for 2 reasons. First, where 2 SufI molecules are bound to TatBC they bind at adjacent sites (Fig. 3*E*). In other words, the second binding site is not randomly selected relative to the first. This pattern of binding would be consistent with 1 region of the TatBC complex being specialized for substrate binding. It would also be consistent with anti-cooperative binding of substrate molecules if the inhibitory effects of substrate binding at a first site are less severe at immediately adjacent sites than at more distal binding sites. By contrast, nonrandom substrate binding is incompatible with a model invoking identical noncooperative binding sites. Second, electron microscopic analysis shows that TatBC complexes with 2 SufI molecules bound are as abundant as TatBC complexes with 1 SufI molecule bound whereas complexes containing >2 SufI molecules are not detected. Such a distribution is not easy to reconcile with substrate binding to equivalent sites but is consistent with the binding sites being of variable affinity. In this context it is worth noting that binding of a single substrate molecule is sufficient to induce structural reorganization of TatBC and that no major additional reorganization of the complex occurs on binding a second molecule of substrate. This correlation suggests that TatBC is designed to respond in a concerted fashion to association with a single substrate molecule and that substrate binding to additional sites is not mechanistically relevant. Concerted structural reorganization would provide a way by which substrate binding at 1 site could alter the affinity of other substrate binding sites. It could also indicate that the whole TatBC complex has to change conformation to allow interaction with TatA.

In complexes containing 2 $SufI_{His}$ molecules the adjacent $SufI_{His}$ molecules are positioned ≈50 ° apart on the circumference of TatBC. Assuming each substrate binding site is formed by a single TatC protomer, and that these protomers are arranged evenly around the TatBC complex, it can be inferred that there are 7 copies of TatC in the substrate-bound TatBC complex. Since TatB and TatC are present at equimolar ratios in the TatBC complex (14), 7 copies of TatB should also be present. This stoichiometry gives a total molecular mass for the substrate-bound complex of approximately 350 kDa which is in good agreement with the mass (≈350 kDa) estimated from the 3-D reconstructions.

Materials and Methods

Sample Production. Plasmid construction, overproduction and purification of $CueO_{His}$, $TatBC_{His}$, and TatBC-$SufI_{His}$, production of TatBC-IMVs, and general protein methods are detailed in *SI Methods*. In vitro reconstitution of TatBC-$CueO_{His}$ complexes was undertaken as follows. One-half milliliter of a 15 mg protein/mL solution of TatBC-IMVs was incubated with 30 μL of a stock ATP regenerating system (giving final concentrations of 2.5 mM ATP, 0.5 mM GTP,

0.5 mM CTP, 0.5 mM UTP, 8 mM creatine phosphate, 40 μg/mL creatine phosphokinase, and 2 mM DTT, pH 7.0) for 15 min at 30 °C. A 2.8 mg protein/mL solution of purified $CueO_{His}$ (0.3 mL) was added and incubation continued for another 30 min. The IMVs were then solubilized by adding an equal volume of 2% (wt/vol) digitonin in 20 mM Mops, pH 7.2, 200 mM NaCl, and 60 mM imidazole, and incubating for 1 h at 4 °C. TatBC-$CueO_{His}$ complexes were purified from the solubilized extract employing the same protocol that was used to isolate the TatBC-$SufI_{His}$ complexes (*SI Methods*).

Transmission Electron Microscopy. Samples of the $TatA_{His}$, $TatBC_{His}$, TatBC-$SufI_{His}$, and TatBC-$CueO_{His}$ preparations with final concentrations of 0.01 mg/mL, 0.015 mg/mL, 0.01 mg/mL, and 0.013 mg/mL, respectively were negatively stained with 2% (wt/vol) uranyl acetate on glow discharged, continuous carbon-coated 300 mesh copper grids (Agar Scientific). Electron micrographs of the $TatA_{His}$, $TatBC_{His}$, and TatBC-$SufI_{His}$ samples were recorded with low dose on Kodak SO-163 electron image film using a Tecnai T12 microscope at 120 kV at a magnification of 42,000 $\times$. Tilt pairs were collected with the first micrograph at a nominal tilt angle of -50 ° and the second at 0 °. The average defocus was approximately 2 μm for the tilted and 1 μm for the untilted micrographs for $TatA_{His}$ and $TatBC_{His}$ and 1.5 μm for TatBC-$SufI_{His}$. The average defocus was approximately 1 μm for the untilted micrographs of TatBC-$CueO_{His}$. Micrographs were digitized on a Zeiss SCAI scanner at a pixel size of 7 μm, corresponding to 1.667 Å on the specimen. Subsequently, adjacent pixels were 3 $\times$ 3 averaged to yield a pixel size of 5 Å. CCD images of the TatBC-$CueO_{His}$ sample were recorded with low dose on a 4 k $\times$ 4 k Gatan CCD camera using a Tecnai F20 at 200 kV, at a magnification of 68,100$\times$, corresponding to a pixel size of 2.22 Å. Subsequently, adjacent pixels were 2 $\times$ 2 averaged to yield a pixel size of 4.44 Å.

Image Processing. The tilted images of the $TatBC_{His}$ and TatBC-$SufI_{His}$ samples were corrected for the effects of the contrast transfer function (CTF) by phase flipping, taking into account the defocus gradient across the micrographs and the position of each particle. Images of the $TatA_{His}$, $TatBC_{His}$, and TatBC-$SufI_{His}$ samples were processed using SPIDER version 11.12 and 15.06 (32). Three-dimensional reconstruction was performed by the random conical tilt method (26), with some scripts adapted from ones provided by N. Boisset and R. Trujillo. Equivalent particles from tilted and untilted images were identified and selected using the ''tilted particles'' option in WEB (32), and used for determination of the tilt geometry for each micrograph. The particles were windowed into 64 $\times$ 64 pixel boxes for $TatBC_{His}$ and TatBC-$SufI_{His}$, and into 100 $\times$ 100 pixel boxes for $TatA_{His}$, filtered, normalized and centered with reference to a circular mask. To avoid reference bias, the first averages were calculated from the untilted images using reference-free alignment (33) and classification. These class averages were then used as initial references for iterative multireference alignment (32). Then the tilted images were grouped and rotationally aligned according to the classification and in-plane orientations of the untilted images. 3D maps were then calculated for each of the tilted image classes (26). Visually similar 3D maps with high mutual cross-correlation coefficients were aligned and merged. The resolutions of the final 3D maps were determined by Fourier shell correlation with the 0.5 correlation criterion. 3D maps were contoured at thresholds of 1.1–1.5 sigma. The X-ray structure of the SufI monomer (25) was manually fitted into the 3-D maps with Chimera (34).

Particles from the TatBC-$CueO_{His}$ sample were selected from CCD images, windowed into 70 $\times$ 70 pixel boxes using EMAN/BOXER (35), and processed as for the untilted $TatBC_{His}$ and TatBC-$SufI_{His}$ complexes.

ACKNOWLEDGMENTS. We thank Luchun Wang for EM support and David Houldershaw and Richard Westlake for computing support. This work was supported by the Wellcome Trust Studentship Grant 072681/Z/03/Z (to M.T.); equipment grant (H.R.S.); Biotechnology and Biological Sciences Research Council Grants C516144 and D011140, and a studentship (S.C.); and Medical Research Council via a Senior Non-Clinical Fellowship Award (T.P).

1. Berks BC, Palmer T, Sargent F (2003) The Tat protein translocation pathway and its role in microbial physiology. *Adv Microb Physiol* 47:187–254.
2. Lee PA, Tullman-Ercek D, Georgiou G (2006) The bacterial twin-arginine translocation pathway. *Annu Rev Microbiol* 60:373–395.
3. Cline K, Theg SM (2007) The Sec and Tat protein translocation pathways in chloroplasts. In *The Enzymes, Molecular Machines Involved in Protein Transport across Cellular Membranes*, eds Dalbey RE, Koehler C, Tamanoi F (Elsevier, San Diego, CA), Vol. XXV, pp 455–485.
4. Natale P, Brüser T, Driessen AJ (2008) Sec- and Tat-mediated protein secretion across the bacterial cytoplasmic membrane—Distinct translocases and mechanisms. *Biochim Biophys Acta* 778:1735–1756.
5. Berks BC, Palmer T, Sargent F (2005) Protein targeting by the bacterial twin-arginine translocation (Tat) pathway. *Curr Opin Microbiol* 8:174–181.
6. Stevenson LG, *et al.* (2007) Rhomboid protease AarA mediates quorum-sensing in *Providencia stuartii* by activating TatA of the twin-arginine translocase. *Proc Natl Acad Sci USA* 104:1003–1008.
7. Chaddock AM, et al. (1995) A new type of signal peptide: Central role of a twin-arginine motif in transfer signals for the ΔpH-dependent thylakoidal protein translocase. *EMBO J* 14:2715–2722.
8. Berks BC (1996) A common export pathway for proteins binding complex redox cofactors? *Mol Microbiol* 22:393–404.
9. Mould RM, Robinson C (1991) A proton gradient is required for the transport of two lumenal oxygen-evolving proteins across the thylakoid membrane. *J Biol Chem* 266:12189–12193.
10. Weiner JH, et al. (1998) A novel and ubiquitous system for membrane targeting and secretion of cofactor-containing proteins. *Cell* 93:93–101.
11. Sargent F, et al. (1998) Overlapping functions of components of a bacterial Sec-independent protein export pathway. *EMBO J* 17:3640–3650.
12. Bogsch EG, et al. (1998) An essential component of a novel bacterial protein export system with homologues in plastids and mitochondria. *J Biol Chem* 273:18003–18006.
13. Sargent F, Stanley NR, Berks BC, Palmer T (1999) Sec-independent protein translocation in *Escherichia coli.* A distinct and pivotal role for the TatB protein. *J Biol Chem* 274:36073–36082.
14. Bolhuis A, Mathers JE, Thomas JD, Barrett CM, Robinson C (2001) TatB and TatC form a functional and structural unit of the twin-arginine translocase from *Escherichia coli. J Biol Chem* 276:20213–20219.
15. Oates J, et al. (2005) The *Escherichia coli* twin-arginine translocation apparatus incorporates a distinct form of TatABC complex, spectrum of modular TatA complexes and minor TatAB complex. *J Mol Biol* 346:295–305.
16. Orriss GL, et al. (2007) TatBC, TatB, and TatC form structurally autonomous units within the twin arginine protein transport system of *Escherichia coli. FEBS Lett* 581:4091–4097.
17. Cline K, Mori H (2001) Thylakoid ΔpH-dependent precursor proteins bind to a cpTatC-Hcf106 complex before Tha4-dependent transport. *J Cell Biol* 154:719–729.
18. Alami M, et al. (2003) Differential interactions between a twin-arginine signal peptide and its translocase in *Escherichia coli. Mol Cell* 12:937–946.
19. de Leeuw E, et al. (2002) Oligomeric properties and signal peptide binding by *Escherichia coli* Tat protein transport complexes. *J Mol Biol* 322:1135–1146.
20. Gohlke U, et al. (2005) The TatA component of the twin-arginine protein transport system forms channel complexes of variable diameter. *Proc Natl Acad Sci USA* 102:10482–10486.
21. Leake MC, et al. (2008) Variable stoichiometry of the TatA component of the twin-arginine protein transport system observed by *in vivo* single-molecule imaging. *Proc Natl Acad Sci USA* 105:15376–15381.
22. Mori H, Cline K (2002) A twin arginine signal peptide and the pH gradient trigger reversible assembly of the thylakoid ΔpH/Tat translocase. *J Cell Biol* 157:205–210.
23. Dabney-Smith C, Mori H, Cline K (2006) Oligomers of Tha4 organize at the thylakoid Tat translocase during protein transport. *J Biol Chem* 281:5476–5483.
24. Dabney-Smith C, Cline K (2009) Clustering of C-terminal stromal domains of Tha4 homo-oligomers during translocation by the Tat protein transport system. *Mol Biol Cell* 20:2060–2069.
25. Tarry M, et al. (2009) The *Escherichia coli* cell division protein and model Tat substrate SufI (FtsP) localizes to the septal ring and has a multi-copper oxidase-like structure. *J Mol Biol* 386:504–519.
26. Radermacher M, Wagenknecht T, Verschoor A, Frank J (1987) Three-dimensional reconstruction from a single-exposure, random conical tilt series applied to the 50S ribosomal subunit of *Escherichia coli*, *J Microsc* 146:113–136.
27. Singh SK, Grass G, Rensing C, Montfort WR (2004) Cuprous oxidase activity of CueO from *Escherichia coli. J Bacteriol* 186:7815–7817.
28. Roberts SA, et al. (2002) Crystal structure and electron transfer kinetics of CueO, a multicopper oxidase required for copper homeostasis in *Escherichia coli. Proc Natl Acad Sci USA* 99:2766–2771.
29. Cline K, McCaffery M (2007) Evidence for a dynamic and transient pathway through the TAT protein transport machinery. *EMBO J* 26:3039–3049.
30. Gérard F, Cline K (2007) The thylakoid proton gradient promotes an advanced stage of signal peptide binding deep within the Tat pathway receptor complex. *J Biol Chem* 282:5263–5272.
31. Alder NN, Theg SM (2003) Protein transport via the cpTat pathway displays cooperativity and is stimulated by transport-incompetent substrate. *FEBS Lett* 540:96–100.
32. Frank J, et al. (1996) SPIDER and WEB: Processing and visualization of images in 3D electron microscopy and related fields. *J Struct Biol* 116:190–199.
33. Penczek P, Radermacher M, Frank J (1992) Three-dimensional reconstruction of single particles embedded in ice. *Ultramicroscopy* 40:33–53.
34. Pettersen EF, et al. (2004) UCSF Chimera—A visualization system for exploratory research and analysis. *J Comput Chem* 25:1605–1612.
35. Ludtke SJ, Baldwin PR, Chiu W (1999) EMAN: Semiautomated software for high-resolution single-particle reconstructions. *J Struct Biol* 128:82–97.